BeBeC-2018-D15

NOISE QUANTIFICATION WITH BEAMFORMING DECONVOLUTION: EFFECTS OF REGULARIZATION AND BOUNDARY CONDITIONS

Oliver Lylloff[1] and Efren Fernandez-Grande[2]
[1]Aerodynamic Design, Dep. Wind Energy, Technical University of Denmark
Frederiksborgvej 399, 4000, Roskilde, Denmark
[2]Acoustic Technology, Dep. Electrical Engineering, Technical University of Denmark
Ørsted Plads 352, 2800 Kgs. Lyngby, Denmark

ABSTRACT

Delay-and-sum (DAS) beamforming can be described as a linear convolution of an unknown sound source distribution and the microphone array response to a point source, i.e., point-spread function. Deconvolution tries to compensate for the influence of the array response and reveal the true source distribution. Deconvolution is an inverse problem in which measurement noise can become dominant and yield meaningless solutions if the problem is not regularized (typically with Tikhonov regularization or a sparsity constraint). Therefore, the obtained solution estimate depends on the choice of regularization parameter, which in turn is highly problem dependent. Additionally, if sound sources are located near the edges of the computational domain, a discontinuity of sound power occurs that can result in a "ringing" effect in the deconvolved image. To remedy this, various boundary conditions can be assumed to model the sound field behaviour outside the computational domain. In this paper, noise quantification from deconvolution is investigated to better understand the derived effect on absolute noise levels. Using benchmark test cases from the aero-acoustic community, absolute noise levels is obtained from deconvolution and compared to that of the test cases. The effects of regularization and boundary conditions are discussed and practical usage scenarios are given.

1. INTRODUCTION

Delay-and-sum (DAS) beamforming is a popular signal processing technique for localizing aero-acoustic sources. Due to inadequate resolution at low frequencies and grating lobes at high frequencies [1], deconvolution methods can be applied to improve the source localization [2]. The outcome is typically a more precise source localization with the ability to obtain absolute

noise levels from selected regions. Classical deconvolution algorithms, such as DAMAS [3], CLEAN [4], NNLS [5], RL [6, 7] have been shown to produce successful reconstructions [2, 8–10]. However, these algorithms and the reconstructions they produce still have limitations and an extended computational cost is one of the main drawbacks.

The deconvolution problem is typically formulated as a linear least-squares problem that can be readily solved by a number of available algorithms [11]. However, in practical usage scenarios, some care is required to obtain trustworthy and physical solutions. The deconvolution problem is often large, which makes a solution infeasible for some (higher-order) algorithms. Additionally, due to the ill-posed nature of the deconvolution problem, regularization is typically added to avoid solutions dominated by noise [12].

There has been a natural interest from the aero-acoustic community to adopt algorithms that originate from the fields of image deblurring and inverse problems, e.g., [13–18]. While these advances show promising results for the deconvolution problem, it can be difficult to evaluate the reconstructions without a common reference. To promote quantitative assessments of microphone array techniques, standardized test data sets (synthesized and experimental) have recently been made publicly available [19]. The first quantitative comparison of deconvolution algorithms across several different research institutions was given in [20, 21].

The purpose of this work is to investigate how absolute noise levels, derived from beamforming deconvolution, are affected by adding regularization and boundary conditions. The synthetic data set described in [20] is used in this work.

Two common regularization strategies are applied to a deconvolution algorithm: A squared ℓ_2-norm and a sparsity inducing ℓ_1-norm. Combined with 7 different boundary conditions, absolute noise levels are reconstructed and evaluated against the reference spectra that accompanies the test data set. To give a fair comparison between different boundary conditions and regularization terms, a so-called proximal gradient algorithm (FISTA [13, 22]) is chosen to perform the deconvolution task. The theory behind proximal methods originates from convex optimization theory [23] and has the advantage that a single implementation of the deconvolution algorithm can evaluate several different regularization strategies.

The data generation, analysis and figures used for the paper is available online [24] in the spirit of reproducible research.

This paper is organized as follows: In Sec. 2, the problem formulation and beamforming framework is described. The deconvolution problem is then stated and the proximal approach is introduced for adding regularization. The simulation study in Sec. 3 is divided into two cases: the first focuses on boundary conditions, and the second on choice of regularization.

In the following, vectors are denoted by boldface lowercase letters and matrices by boldface uppercase letters.

2. BEAMFORMING DECONVOLUTION

Consider the sound pressure measured using a microphone array with M microphones due to a single point source located at $\mathbf{r}_s$. Assuming free-field conditions and no flow, the sound pressure at the m'th microphone, $\mathbf{r}_m$, is,

$$p(\mathbf{r}_m) = \frac{q(\mathbf{r}_s)}{|\mathbf{r}_s - \mathbf{r}_m|} e^{-jk|\mathbf{r}_s - \mathbf{r}_m|} \tag{1}$$

where q is the strength of the source, $|\mathbf{r}_s - \mathbf{r}_m|$ is the distance from the sound source to the m'th microphone, and k is the wave number [25]. By collecting the sound pressure from all microphones and arranging them in a vector $\mathbf{p} \equiv [p(\mathbf{r}_1), p(\mathbf{r}_2), \ldots, p(\mathbf{r}_M)]^T$, and computing the cross spectral matrix $\mathbf{C} \equiv E\{\mathbf{p}\mathbf{p}^H\}$, the mean-squared beamforming output for a focus point $\mathbf{r}_f$ is given by,

$$b(\mathbf{r}_f) = \mathbf{v}(\mathbf{r}_f)^H \mathbf{C} \mathbf{v}(\mathbf{r}_f) \tag{2}$$

where $\mathbf{v}(\mathbf{r}_f)$ is a steering vector that contains transfer functions from the microphone array to the focus point, $(\cdot)^H$ is the hermitian transpose, and $E\{\cdot\}$ is the expectation operator. Computing the real part of Eq. (2) for all focus points in the area of interest produces a beamforming map.

The formulation of the steering vector $\mathbf{v}$ can be found in different variations in the literature. In [26] four variants are collected and identified that can either reconstruct the source position or level correctly. In this work, formulation III, that was found to reconstruct the level correctly, is used,

$$v_m(\mathbf{r}_f) = \frac{e^{-jk\left(|\mathbf{r}_f - \mathbf{r}_m| - |\mathbf{r}_f - \mathbf{r}_0|\right)}}{|\mathbf{r}_f - \mathbf{r}_0||\mathbf{r}_f - \mathbf{r}_m| \sum_{j=1}^{N} |\mathbf{r}_f - \mathbf{r}_j|^{-2}}. \tag{3}$$

Assuming incoherent sources, the cross-spectral matrix $\mathbf{C}$ can be modelled as

$$\tilde{\mathbf{C}} = \sum_{n=1}^{N^2} \overline{|q|^2} \cdot \mathbf{v}(\mathbf{r}_n)\mathbf{v}(\mathbf{r}_n)^H, \tag{4}$$

where $\overline{(\cdot)}$ is the spectral average. The beamforming output in Eq. (2) can thus be modelled as

$$b(\mathbf{r}_f) = \sum_{n=1}^{N^2} \overline{|q|^2} \cdot \mathrm{PSF}(\mathbf{r}_f, \mathbf{r}_n) \tag{5}$$

where n is the n'th grid point in a $N \times N$ computational grid, PSF is the beamforming output due to a unit-power point source, i.e., point-spread function,

$$\mathrm{PSF}(\mathbf{r}_f, \mathbf{r}_n) = \mathbf{v}(\mathbf{r}_f)^H \left[\mathbf{v}(\mathbf{r}_n)\mathbf{v}(\mathbf{r}_n)^H\right] \mathbf{v}(\mathbf{r}_f). \tag{6}$$

The PSF array, $\mathbf{P}$, is the matrix, or image, of a source placed in a particular grid point $\mathbf{r}_n$. Computing $\mathbf{P}$ for all grid points and stacking them column-wise produces the blurring matrix $\mathbf{A}$ with dimensions $N^2 \times N^2$. If the point-spread function is shift-invariant, Eq. (5) is modified to

$$b(\mathbf{r}_f) = \sum_{n=1}^{N^2} \overline{|q|^2} \cdot \mathrm{PSF}(\mathbf{r}_f - \mathbf{r}_n) \tag{7}$$

which corresponds to a linear convolution of the source distribution and a single point-spread function. The PSF array, $\mathbf{P}$, is then only computed for a source located at the centre of the domain and the blurring matrix $\mathbf{A}$ is a block Toeplitz with Toeplitz blocks (BTTB) matrix. It is known that the Fast Fourier Transform can be used to efficiently compute matrix vector products $\mathbf{A}\mathbf{x}$ without forming $\mathbf{A}$ explicitely [12].

The deconvolution problem is given by,

$$\underset{\mathbf{x}\in\mathbb{R}^{N\times N}}{\text{minimize}} \quad \tfrac{1}{2}\|\mathbf{Aq}-\mathbf{b}\|_2^2, \tag{8}$$

where $\mathbf{q} = \left[|q_1|^2, |q_2|^2, \ldots, |q_{N^2}|^2\right]$, $\mathbf{Aq}$ is a two-dimensional convolution product computed by $\mathcal{F}^{-1}\left[\mathcal{F}(\mathbf{q}) \odot \mathcal{F}(\mathbf{P})\right]$, where $\mathcal{F}$ and $\mathcal{F}^{-1}$ is the 2D Fourier Transform operator and its inverse, and $(\odot)$ is the element-wise product. The computational advantage comes from the fact that the convolution $\mathbf{Aq}$ can be performed by the Fast Fourier Transform without forming the blurring matrix $\mathbf{A}$. Due to its periodic nature, padding is required to avoid wrap-around errors [27]. This padding impose a boundary condition on the beamforming map, i.e., the assumed behaviour of the sound field outside the field of view. The derived effect of boundary conditions on reconstructed noise levels are the focus of this paper.

2.1. The Proximal Approach

The optimization problem stated in Eq. (8) is convex, which means that if a minimum of the deconvolution problem can be found it is guaranteed to be a global minimum of the optimization problem [28].

The starting point in Eq. (8) can provide useful reconstructions, however, a non-negativity constraint is typically added to the optimization problem due to the non-negative source powers, $\mathbf{q}$,

$$\begin{aligned} &\underset{\mathbf{q}\in\mathbb{R}^{N\times N}}{\text{minimize}} \quad \tfrac{1}{2}\|\mathbf{Aq}-\mathbf{b}\|_2^2 + I_+(\mathbf{q}) \\ &\text{where} \quad I_+(\mathbf{q}) = \begin{cases} 0, & \text{if } q \in \mathbb{R}_+^n \\ \infty, & \text{otherwise,} \end{cases} \end{aligned} \tag{9}$$

where $\mathbb{R}_+^n$ is the non-negative orthant [28]. This formulation is equivalent to the non-negative least squares problem NNLS [2, 5]. What is clear from this formulation is that the objective function is no longer differentiable and deconvolution algorithms that depend on the first or second derivative will break.

With the proximal approach, the optimization problem is split into differentiable and non-differentiable parts. The proximal operator of a non-differentiable function g, is given by

$$\text{prox}_g(v) = \underset{x}{\text{argmin}} \left(g(x) + \tfrac{1}{2}\|x-v\|_2^2\right). \tag{10}$$

$\text{prox}_g(v)$ can be interpreted as a point that compromises between minimizing g and being near v [23]. For example, the proximal operator of the indicator function in Eq. (9) is the Euclidean projection of $\mathbf{q}$ onto $\mathbb{R}_+^n$, i.e., $\max(0, \mathbf{q})$.

With this framework in place, it is possible to introduce additional variations of the optimization problem (9). In this work, two well-known formulations will be applied, namely a squared ℓ_2-norm regularization term

$$\underset{\mathbf{q}\in\mathbb{R}^{N\times N}}{\text{minimize}} \quad \tfrac{1}{2}\|\mathbf{Aq}-\mathbf{b}\|_2^2 + \lambda\|\mathbf{q}\|_2^2 + I_+(\mathbf{q}) \tag{11}$$

which is a constrained variation of Tikhonov regularization [29], and a ℓ_1-norm regularization term,

$$\underset{\mathbf{q}\in\mathbb{R}^{N\times N}}{\text{minimize}} \quad \tfrac{1}{2}\|\mathbf{A}\mathbf{q}-\mathbf{b}\|_2^2+\lambda\|\mathbf{q}\|_1+I_+(\mathbf{q}), \tag{12}$$

which induce sparse solutions and is similar to compressive sensing or LASSO [30]. Other interesting variations that is straight-forward to implement with the proximal approach, include the edge-preserving Total Variation Denoising [31] and Elastic Net [18].

The deconvolution algorithm, which is used in this study, is based on a fast proximal gradient algorithm, FISTA [22], that has been applied to beamforming deconvolution in [13] and extended in [14, 32].

2.2. Boundary Conditions

Boundary conditions model the behaviour of the beamforming map outside the field of view [33]. Consider for instance the simple example of a 3×3 matrix $\mathbf{X}$,

$$\mathbf{X}=\begin{bmatrix}1&2&3\\4&5&6\\7&8&9\end{bmatrix}.$$

The most common boundary condition is a zero boundary condition. When applied to $\mathbf{X}$, the matrix is embedded into a larger matrix padded with zeros,

$$\mathbf{X}_{\text{zeroBC}}=\begin{bmatrix}\mathbf{0}&\mathbf{0}&\mathbf{0}\\\mathbf{0}&\mathbf{X}&\mathbf{0}\\\mathbf{0}&\mathbf{0}&\mathbf{0}\end{bmatrix}.$$

This boundary condition is a common choice when performing convolutions via the Fast Fourier Transform [27]. If the beamforming map is confined to the centre and nearly zero at the edges, a zero boundary condition might be a realistic model of the behaviour outside the field of view. However, if the beamforming map is nonzero, as is often the case at low frequencies, the sound power "spills over the edge" of the computational domain and a discontinuity occurs that can affect the reconstructed sound map. Four common choices of boundary conditions are shown in Fig. 10.

An additional boundary condition is proposed in this work, the extended BC, that simply requires a re-computation of the beamforming map in an extended computational domain that is larger than the original. The "padding" in this case is just the computed extension of the beamforming map and thus relieves sharp discontinuities at the edge. In all cases, the padding is removed after deconvolution to the region of interest.

3. SIMULATION STUDY

In this study, a synthetic test case of four incoherent point sources are considered (Benchmark 7: Four Monopole Sources [19]). The sources are arranged in a square with side lengths of 0.2 m and a microphone array with 64 microphones is placed at a distance of 0.75 m (see Fig.

1). There are two subcases included in the data set: subcase a, all sources have equal power, and subcase b, where the sources have different power. Reference spectra of each source are included in the data set and the reconstructed sound maps presented in the following are evaluated against the reference by the level difference $\Delta L = L - L_{\text{ref}}$ for each individual frequency bin. The reconstructed levels are estimated by a spatial integration over a square with a side length of 0.1 m centered at the nominal source position.

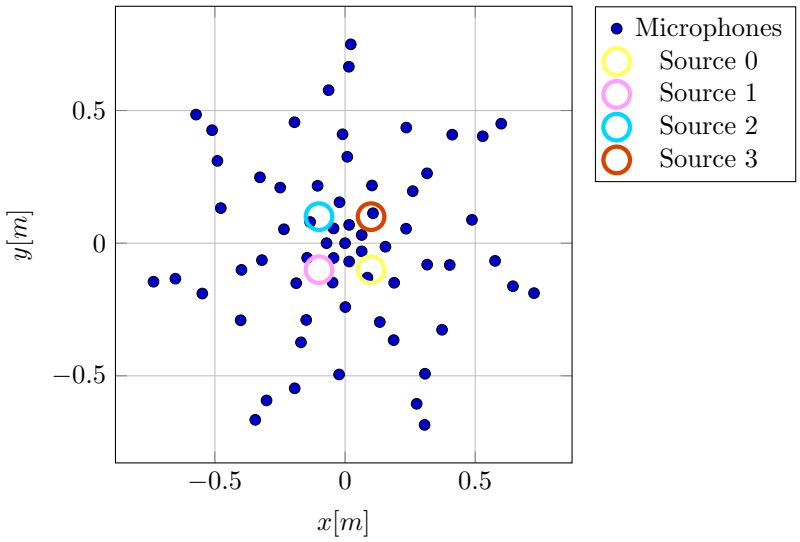

Figure 1: Geometry of the setup.

3.1. Case I: Boundary Conditions

The purpose of this case is to analyse the effects of boundary conditions at low frequencies when the beamforming map has a wide mainlobe and a large discontinuity appears at the edge. Four monopoles with equal power (Benchmark 7, subcase a [19]) is reconstructed from beamforming maps at 7 frequencies $f = [700, 800, 1000, 1500, 2000, 2500, 5000]$ Hz, each with a bin width of 50 Hz. Additionally, 6 different boundary conditions (and one without) is applied to the beamforming maps, this gives a total of 49 reconstructions. The computational domain is restricted to $x = y = [-0.2; 0.2]$ m and the measurement distance is $z = 0.75$ m. The maximum number of iterations with the deconvolution algorithm is set to 3000.

Beamforming maps padded to size $(2N-1) \times (2N-1)$ by 6 different boundary conditions (zero, replicate, symmetric, periodic, reflect, and the proposed extended BC) are shown in Fig. 2. Due to the symmetry of the source distribution, the symmetric, periodic, and reflect boundary conditions, coincide and have similar appearances. The beamforming maps at $f = 1000$ Hz and $f = 1500$ Hz are shown in Fig. 3. From a visual inspection, the four sources are barely separated at $f = 1500$ Hz, and at $f = 1000$Hz it is no longer possible to identify them.

The reconstructed source levels for Source 3 are shown in Table 1. For the sake of brevity, results for the remaining sources, which is very similar, are omitted. All reconstructions at and above 1500 Hz show small level deviations from the reference within ± 1 dB. Below 1500 Hz, only the extended boundary condition, is capable of reconstructing the source level correctly.

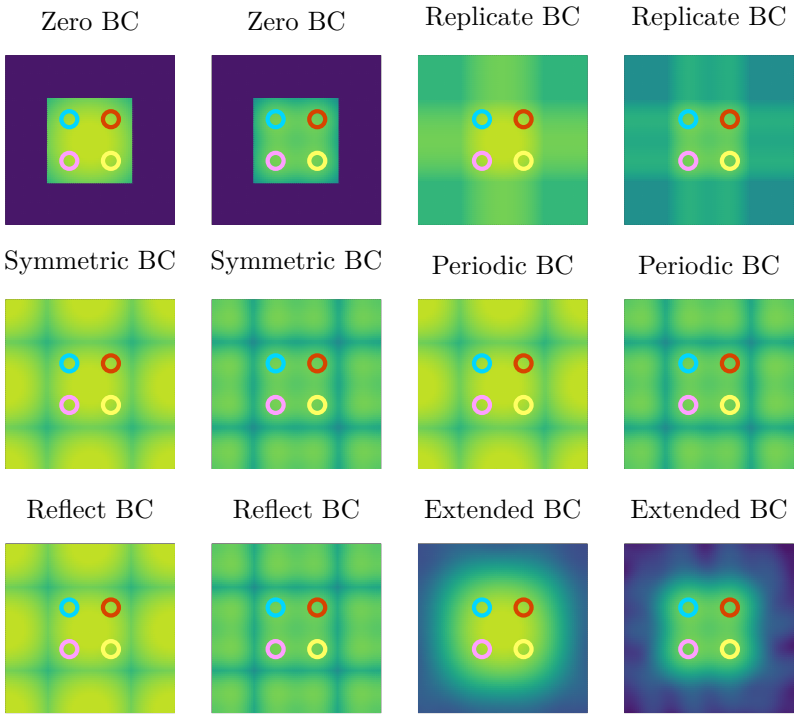

Figure 2: Padded beamforming maps at 1000 Hz (left of each pair) and 1500 Hz (right of each pair). The area of interest is $x = y = [-0.2; 0.2]$ m padded to $x = y = [-0.4; 0.4]$ m and the dynamic range is 18 dB.

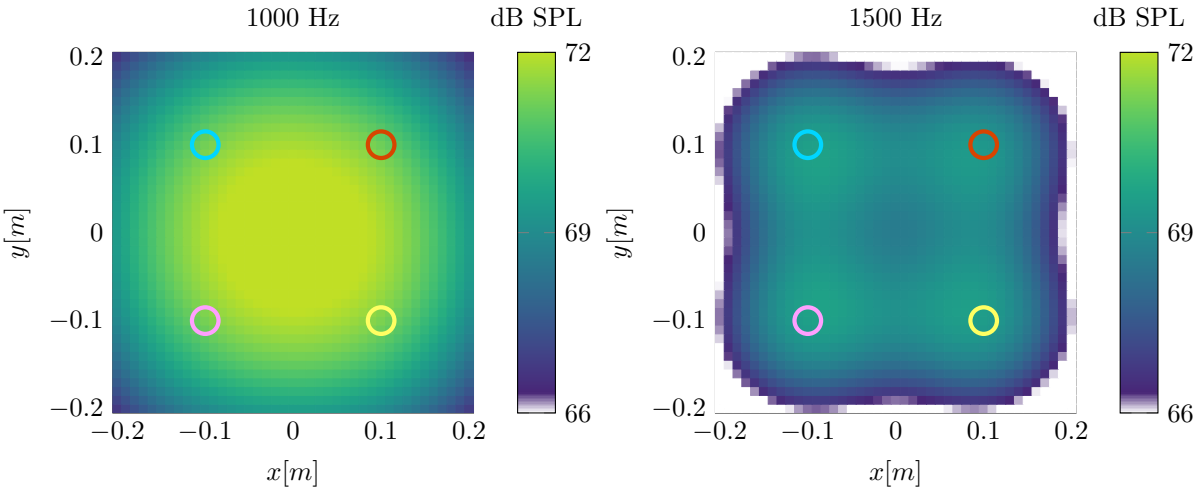

Figure 3: Case I: Beamforming maps at $f = 1000$Hz and $f = 1500$ Hz. Circles indicate positions of point sources.

Surprisingly, the no BC case, without any padding, performs as well as the other cases. Reconstructed source maps for two boundary conditions (zero BC and extended BC) are shown in Fig. 4. Again, for the sake of brevity, only two reconstructions are shown. The remaining re-

Table 1: Level differences (Source 3) from reference $\Delta L = L - L_{ref}$ [dB]. (–): no data.

f [Hz]	700	800	1000	1500	2000	2500	5000
no BC	–	–	–	0.1	0.7	0.8	0.9
zero BC	–	–	–	0.5	0.8	0.9	0.7
replicate BC	–	–	–	0.5	0.8	0.9	0.8
symmetric BC	–	–	–	0.0	0.6	0.8	0.9
periodic BC	–	–	–	0.0	0.7	0.8	0.9
reflect BC	–	–	–	-0.1	0.6	0.8	0.8
extended BC	–	0.8	0.8	0.6	0.7	0.8	0.7

constructions are very similar to the zero BC case. Upon inspection of the reconstructed maps (Fig. 4), it is clear that the reconstructions become useless below a certain frequency limit. This cut-off frequency occurs around 800 Hz for the extended BC but for all other boundary conditions it is around 1500 Hz.

The Rayleigh criterion is commonly used as a measure of resolution and describes the smallest angular separation at which two sources can be separated [34],

$$R \approx 1.22 \frac{L}{D} \lambda, \tag{13}$$

where L is the (on axis) measurement distance, D is the array aperture and λ the wavelength. The resolution as function of frequency for this specific case, with $L = 0.75$m and $D = 1.5$m is shown in Fig. 5.

At the cut-off frequency of the extended BC, 800 Hz, the resolution is approximately 0.26 m and at 1500 Hz, which is the cut-off frequency of the remaining boundary conditions, the resolution is approximately 0.14 m. These numbers indicate that there is a relationship between resolution, cut-off frequency and boundary condition. The shortest distance from a source to the edge of the unpadded beamforming map is 0.1 m, except for the case of extended BC, that is padded with the natural extension of the beamforming map, where the shortest distance is 0.3 m. One possible explanation is that when the resolution is too low, the sources cannot be separated from edge and deconvolution fails to reconstruct correctly. The cut-off frequency due to that interpretation is from Eq. (13),

$$f_{\text{min}} = 1.22 \frac{L}{D} \frac{c}{R_{\text{min}}}, \tag{14}$$

where c is the speed of sound and R_{min} is the shortest distance from a source to the edge of the beamforming map. For $R_{\text{min}} = 0.1, f_{\text{min}} = 2092$Hz. This estimate is much higher than what was found empirically above. The cut-off frequency in Eq. (14) can serve as a rule of thumb for a lower frequency limit of deconvolution given certain boundary conditions, however, it is still based on the Rayleigh criterion which is a convenient reference point for resolution rather than a strict physical limit [35].

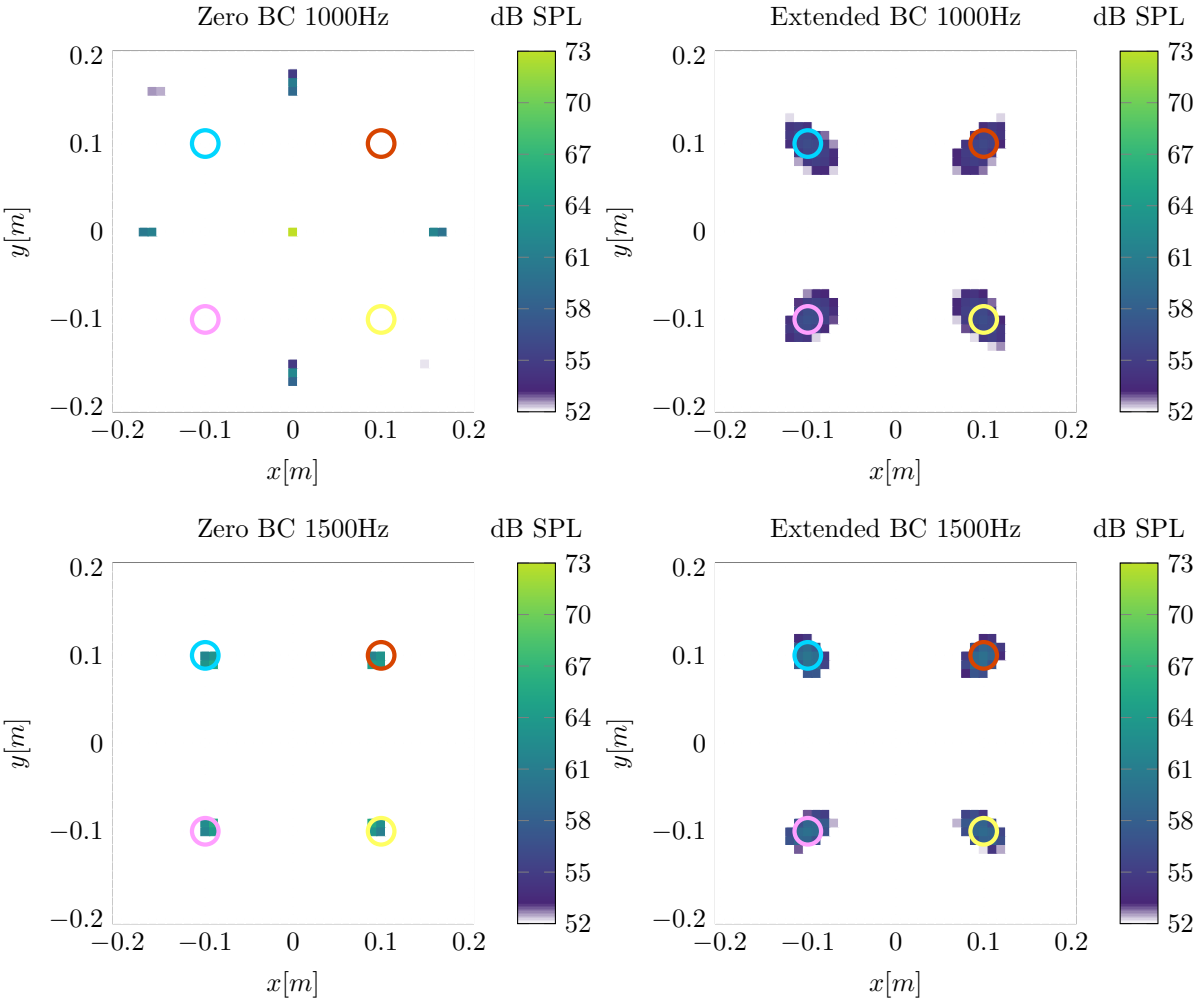

Figure 4: Case I: Reconstructed source maps at $f = 1000Hz$ and $f = 1500$ Hz. Circles indicate positions of point sources.

3.2. Case II: Regularization

The purpose of this case is to investigate the effects of regularization on absolute noise levels. Similar to Case I (Sec. 3.1), four monopole sources are considered, however, now subcase b from [19] is used, where the source powers are different. Source 0 is the strongest, Source 1 is -6dB below, Source 2 is -12 dB below Source 0, and Source 3 is -18dB below Source 0. The source levels are reconstructed from beamforming maps at frequencies $f = [500, 550, \ldots, 11250]$ Hz with a bin width of 50 Hz. Two regularization terms are added: a ℓ_1-norm and ℓ_2-norm term defined in Eq. (11) and (12), respectively, each with 20 different regularization parameters in the range $\lambda = [10^{-5}; 10^{2}]$. The domain of interest is $x = y = [-0.5; 0.5]$, which gives a cut-off frequency $f_{\text{min}} = 523$ Hz according to Eq. (14). A zero boundary condition is chosen since it was found in Case I that, above the cut-off frequency, all boundary conditions could reconstruct absolute noise levels equally well. The maximum number of iterations with the deconvolution algorithm is again set to 3000.

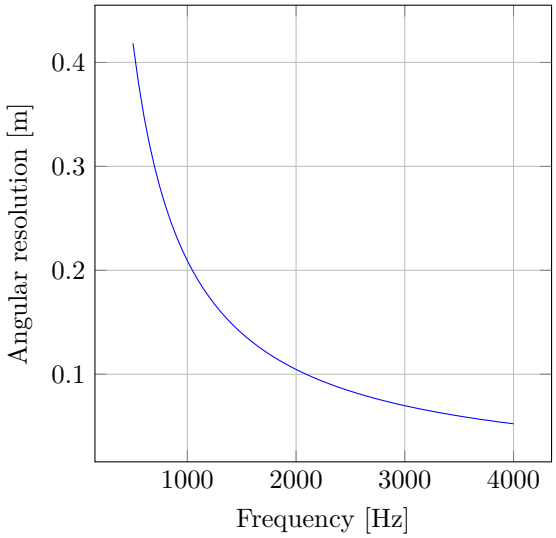

Figure 5: Resolution due to the Rayleigh criterion.

The beamforming maps at $f = 1000$ Hz and $f = 1500$ Hz are shown in Fig. 6 and a comparison between the reconstructions with the two regularization methods are shown in Fig. 7. As expected, the ℓ_1-norm method induce a more sparse reconstruction than the ℓ_2-norm. By visual inspection it seems that only two sources are identified properly by the ℓ_1-norm method whereas three is identified by the ℓ_2-norm method.

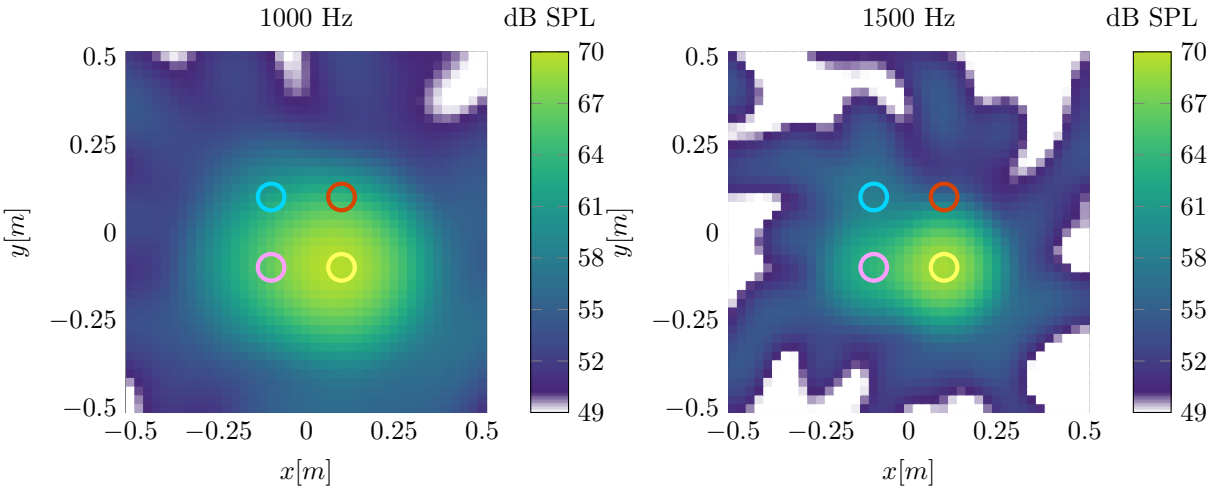

Figure 6: Case II: Beamforming maps at $f = 1000Hz$ and $f = 1500$ Hz. Circles indicate positions of point sources.

The deconvolution problem is solved for every regularization parameter and regularization method in the frequency range of interest. Level differences ΔL are computed by comparing the reconstruction level of each source, determined via spatial integration, with the reference levels from the data set. Figure 8 shows ΔL as function of regularization parameter for 1500Hz and

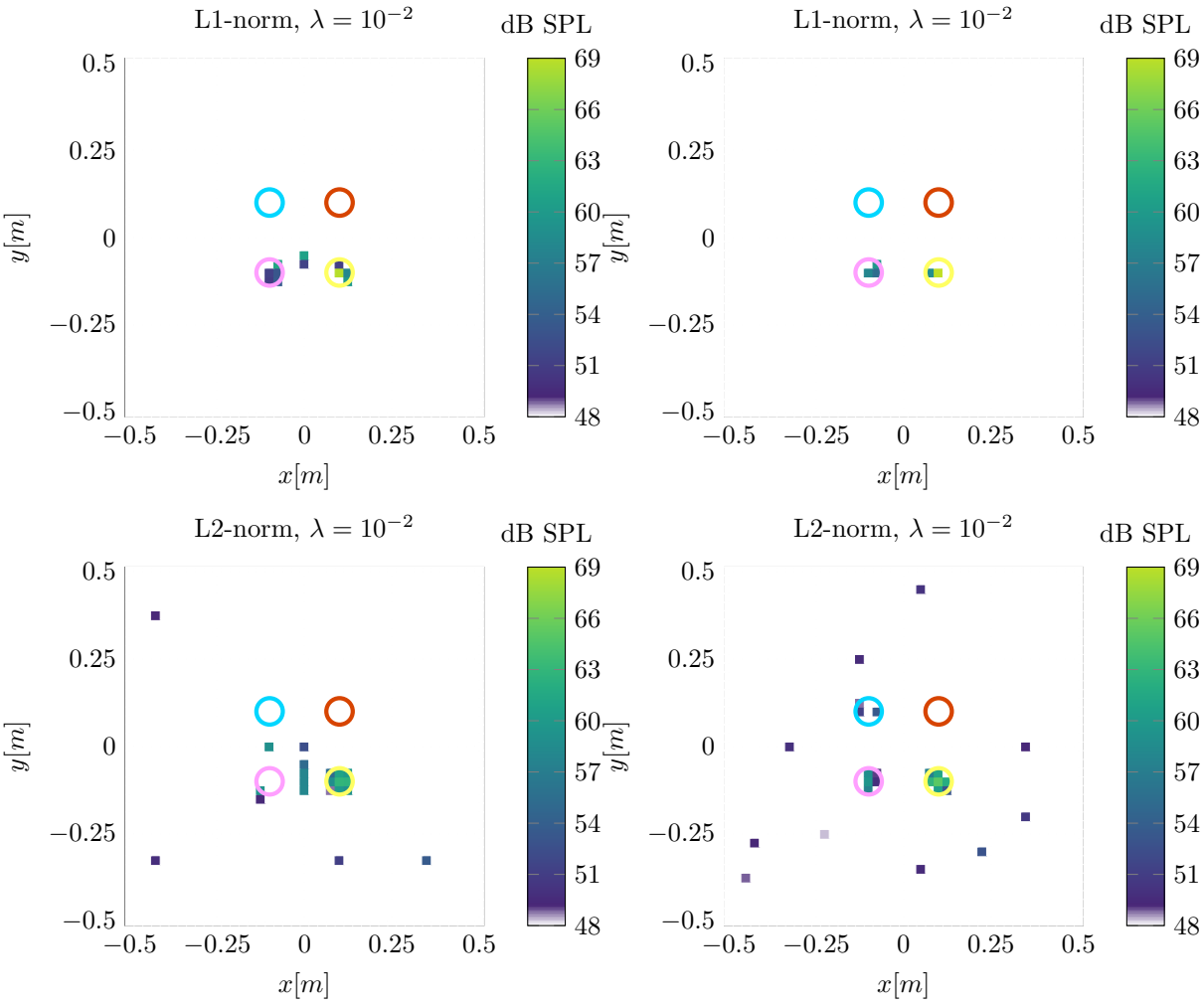

Figure 7: Case II: Reconstructed source maps at $f = 1000Hz$ (left) and $f = 1500Hz$ (right) with ℓ_1-norm and ℓ_2-norm regularization. Circles indicate positions of point sources.

3000Hz. From this it is clear that both methods can actually identify three of the four sources but due to the chosen regularization parameter, $\lambda = 10^{-2}$, only two is visible with the ℓ_1-norm method at 1500 Hz.

For small λ values ($< 10^{-4}$), both regularization methods perform well in terms of reconstructed sound levels. This is not an observation that holds in general. The data set has a high signal-to-noise ratio and regularization is not required to obtain good reconstructions. For real-world problems, measurement noise will in general require a need for regularization. For larger values of λ more emphasis is put on the regularization term and both methods display knee-points at which the reconstruction level drops significantly. The λ value at which this point occurs seems to depend on both frequency and signal-to-noise ratio.

The stronger the source, the larger is λ at the knee-point. This behaviour is in line with one of the main drawbacks of ℓ_1-norm regularization: When λ increases, the source distribution becomes increasingly more sparse and sound power is aggregated around fewer points. The

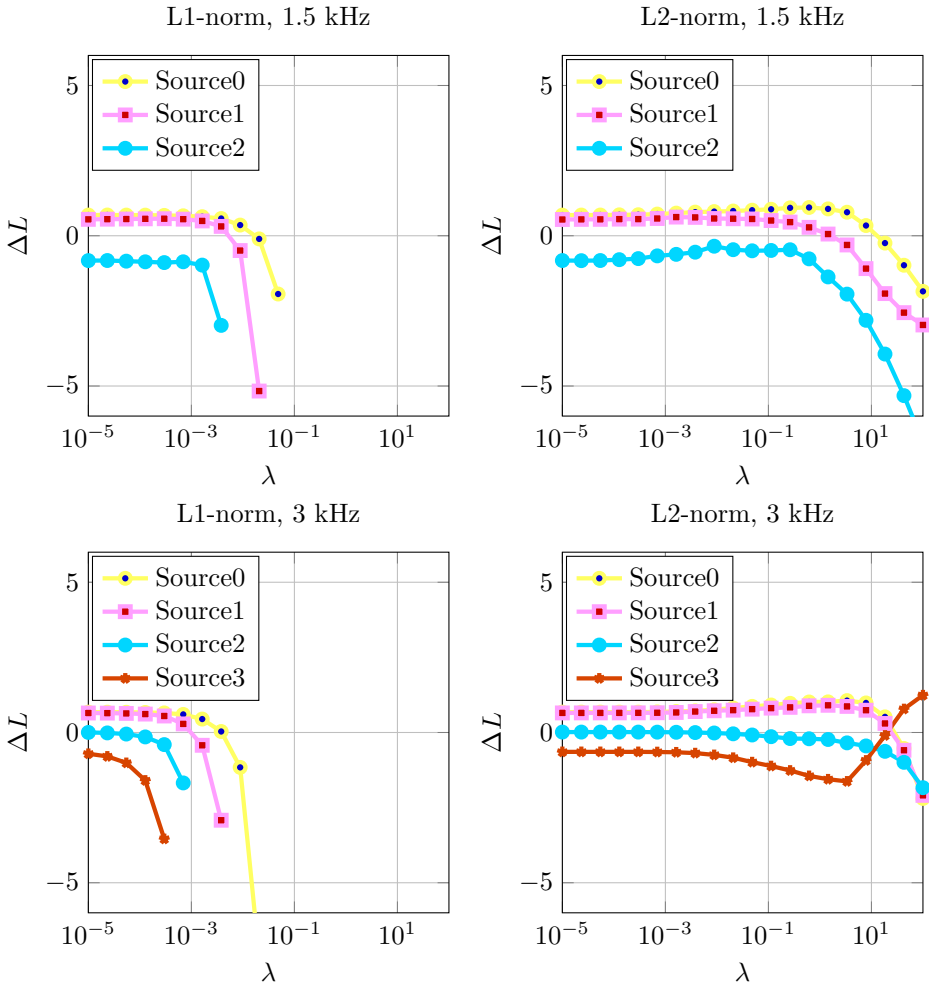

Figure 8: Case II: Level differences for the four sources at $f = 1500$ Hz (above) and $f = 3000$ Hz (below) as function of λ.

sound power of the weakest sources is absorbed into the stronger ones.

Increasing the frequency seems to move the knee-point towards lower λ. This pattern is most clear for ℓ_1-norm regularization. On possible explanation for the behaviour has to do with the complexity of the underlying model, i.e., point-spread function. The width of the mainlobe of the point-spread function increases as the frequency decrease. This means, that the number of linearly independent rows/columns in the point-spread function, i.e., matrix rank, decrease with frequency, thus the complexity decreases. With lower complexity, a larger regularization is required to induce sparsity.

Using the reference levels from the data set, optimal regularization parameters can be found from the reconstructions. The optimal λ is determined for each frequency to be the largest one that gives a reconstruction level within ± 2 dB of the reference, $|\Delta L| < 2$ dB. These values are shown in Fig. 9 for the two regularization methods. The behaviour of the ℓ_1-norm method is in line with the observation from Fig. 8: λ increases with decreasing frequency and a clear divide is seen between the sources. The ℓ_1-norm regularization can reconstruct absolute noise levels

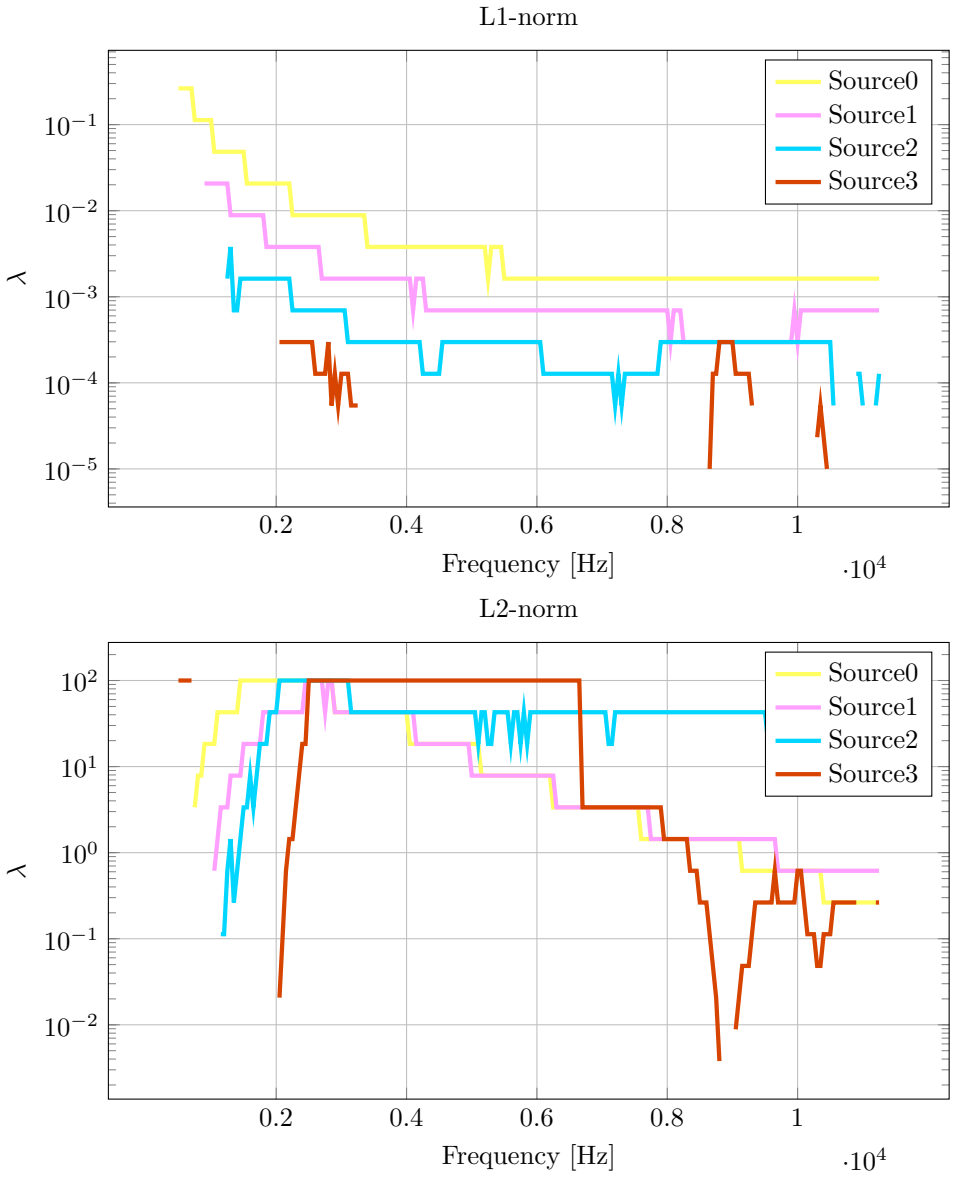

Figure 9: Case II: Optimal λ values as function of frequency for ℓ_1-norm (above) and ℓ_2-norm (below).

within ± 2 dB for all but the weakest source in the range from 500 Hz to approximately 10 kHz. The ℓ_2-norm regularization seems better at reconstructing absolute levels for the weakest source, however, by inspection of the deconvolved maps (omitted here for brevity), the resolution is very low and not useful for source localization.

4. CONCLUSIONS

Absolute noise levels have been reconstructed with beamforming deconvolution and the effects of boundary conditions and regularization have been evaluated against the reference levels.

Seven different boundary conditions have been applied, six of them commonly seen in the deblurring literature, and it has been found that they all give rise to good reconstructions of absolute noise levels within ± 1 dB of the reference. A lower frequency limit has been proposed, based on the Rayleigh criterion, below which deconvolution fails to reconstruct the source distribution. The results indicate that the use of an extended BC extends the frequency range in which deconvolution can successfully be applied at low frequencies.

Two common regularization terms have been investigated and the importance of a correctly chosen regularization parameter has been reviewed. Specifically, the ℓ_1-norm regularization has been observed to have a clear dependency on frequency and signal-to-noise ratio. Further investigations are required before a general recommendation for regularization parameter estimation can be derived.

This study has been based on results generated by a single deconvolution algorithm using a single data set. Using the same methodology as presented, future investigations should take into account other algorithms and data sets to get a more general picture of boundary and regularization effects on the noise quantification problem.

A. Appendix

Reflect

$$\left[\begin{array}{ccc|ccc|ccc}
5 & 6 & 5 & 4 & 5 & 6 & 5 & 4 & 5 \\
8 & 9 & 8 & 7 & 8 & 9 & 8 & 7 & 8 \\
5 & 6 & 5 & 4 & 5 & 6 & 5 & 4 & 5 \\
\hline
2 & 3 & 2 & 1 & 2 & 3 & 2 & 1 & 2 \\
5 & 6 & 5 & 4 & 5 & 6 & 5 & 4 & 5 \\
8 & 9 & 8 & 7 & 8 & 9 & 8 & 7 & 8 \\
\hline
5 & 6 & 5 & 4 & 5 & 6 & 5 & 4 & 5 \\
2 & 3 & 2 & 1 & 2 & 3 & 2 & 1 & 2 \\
5 & 6 & 5 & 4 & 5 & 6 & 5 & 4 & 5
\end{array}\right]$$

Replicate

$$\left[\begin{array}{ccc|ccc|ccc}
1 & 1 & 1 & 1 & 2 & 3 & 3 & 3 & 3 \\
1 & 1 & 1 & 1 & 2 & 3 & 3 & 3 & 3 \\
1 & 1 & 1 & 1 & 2 & 3 & 3 & 3 & 3 \\
\hline
1 & 1 & 1 & 1 & 2 & 3 & 3 & 3 & 3 \\
4 & 4 & 4 & 4 & 5 & 6 & 6 & 6 & 6 \\
7 & 7 & 7 & 7 & 8 & 9 & 9 & 9 & 9 \\
\hline
7 & 7 & 7 & 7 & 8 & 9 & 9 & 9 & 9 \\
7 & 7 & 7 & 7 & 8 & 9 & 9 & 9 & 9 \\
7 & 7 & 7 & 7 & 8 & 9 & 9 & 9 & 9
\end{array}\right]$$

Symmetric

$$\left[\begin{array}{ccc|ccc|ccc}
9 & 8 & 7 & 7 & 8 & 9 & 9 & 8 & 7 \\
6 & 5 & 4 & 4 & 5 & 6 & 6 & 5 & 4 \\
3 & 2 & 1 & 1 & 2 & 3 & 3 & 2 & 1 \\
\hline
3 & 2 & 1 & 1 & 2 & 3 & 3 & 2 & 1 \\
6 & 5 & 4 & 4 & 5 & 6 & 6 & 5 & 4 \\
9 & 8 & 7 & 7 & 8 & 9 & 9 & 8 & 7 \\
\hline
9 & 8 & 7 & 7 & 8 & 9 & 9 & 8 & 7 \\
6 & 5 & 4 & 4 & 5 & 6 & 6 & 5 & 4 \\
3 & 2 & 1 & 1 & 2 & 3 & 3 & 2 & 1
\end{array}\right]$$

Periodic

$$\left[\begin{array}{ccc|ccc|ccc}
1 & 2 & 3 & 1 & 2 & 3 & 1 & 2 & 3 \\
4 & 5 & 6 & 4 & 5 & 6 & 4 & 5 & 6 \\
7 & 8 & 9 & 7 & 8 & 9 & 7 & 8 & 9 \\
\hline
1 & 2 & 3 & 1 & 2 & 3 & 1 & 2 & 3 \\
4 & 5 & 6 & 4 & 5 & 6 & 4 & 5 & 6 \\
7 & 8 & 9 & 7 & 8 & 9 & 7 & 8 & 9 \\
\hline
1 & 2 & 3 & 1 & 2 & 3 & 1 & 2 & 3 \\
4 & 5 & 6 & 4 & 5 & 6 & 4 & 5 & 6 \\
7 & 8 & 9 & 7 & 8 & 9 & 7 & 8 & 9
\end{array}\right]$$

Figure 10: Common boundary conditions imposed on matrix $\mathbf{X}$.

References

[1] J. Hald. "Beamforming and Wavenumber Processing". *Handbook of Signal Processing in Acoustics*. Ed. by D. Havelock, S. Kuwano, and M. Vorländer. New York, NY: Springer New York, 2008, pp. 131–144. DOI: 10.1007/978-0-387-30441-0_9.

[2] K. Ehrenfried and L. Koop. "Comparison of Iterative Deconvolution Algorithms for the Mapping of Acoustic Sources". *AIAA Journal* 45.7 (2007), pp. 1584–1595. DOI: 10.2514/1.26320.

[3] T. F. Brooks and W. M. Humphreys. "A deconvolution approach for the mapping of acoustic sources (DAMAS) determined from phased microphone arrays". *Journal of Sound and Vibration* 294.4-5 (2006), pp. 856–879.

[4] J. A. Högbom. "Aperture synthesis with a non-regular distribution of interferometer baselines". *Astronomy and Astrophysics Supplement Series* 15.3 (1974), pp. 417–426.

[5] C. Lawson and R. Hanson. *Solving Least Squares Problems*. Society for Industrial and Applied Mathematics, 1995. DOI: 10.1137/1.9781611971217.

[6] W. H. Richardson. "Bayesian-based iterative method of image restoration". *Journal of the Optical Society of America* 62.1 (1972), pp. 55–59.

[7] L. B. Lucy. "An iterative technique for the rectification of observed distributions". *Astronomical Journal* 79 (1974), p. 745.

[8] T. Yardibi et al. "Comparison of Microphone Array Processing Techniques for Aeroacoustic Measurements". *International Journal of Aeroacoustics* 9.6 (2010), pp. 733–761. DOI: 10.1260/1475-472X.9.6.733.

[9] Z. Chu and Y. Yang. "Comparison of deconvolution methods for the visualization of acoustic sources based on cross-spectral imaging function beamforming". *Mechanical Systems and Signal Processing* 48.1 (2014), pp. 404–422. DOI: 10.1016/j.ymssp.2014.03.012.

[10] Q. Leclère. "A Unified Formalism For Acoustic Imaging Techniques: Illustrations in the Frame of a Didactic Numerical Benchmark". *Proceedings of the 6th Berlin Beamforming Conference*. Feb. 2016.

[11] Å. Björck. *Numerical Methods for Least Squares Problems*. Society for Industrial and Applied Mathematics, 1996. DOI: 10.1137/1.9781611971484.

[12] P. Hansen. *Discrete Inverse Problems*. Society for Industrial and Applied Mathematics, 2010. DOI: 10.1137/1.9780898718836.

[13] O. Lylloff et al. "Improving the efficiency of deconvolution algorithms for sound source localization". *Journal of the Acoustical Society of America* 138.1 (2015), pp. 172–180. DOI: 10.1121/1.4922516.

[14] "Periodic boundary based FFT-FISTA for sound source identification". *Applied Acoustics* 130 (2018), pp. 87–91. DOI: 10.1016/j.apacoust.2017.09.009.

[15] L. Hoeltgen et al. "Sparse l1 Regularisation of Matrix Valued Models for Acoustic Source Characterisation". *arXiv.org* (July 2016). arXiv: 1607.00171v1.

[16] J. Antoni. "A Bayesian approach to sound source reconstruction: Optimal basis, regularization, and focusing". *The Journal of the Acoustical Society of America* 131.4 (2012), pp. 2873–2890. DOI: 10.1121/1.3685484.

[17] A. Xenaki, P. Gerstoft, and K. Mosegaard. "Compressive beamforming". *The Journal of the Acoustical Society of America* 136.1 (2014), pp. 260–271. DOI: 10.1121/1.4883360.

[18] X. Li, W. Tong, and M. Jiang. "Sound Source Localizarion Via Elastic Net Regularization". *Proceedings of the 5th Berlin Beamforming Conference*. 2014.

[19] *Benchmarking Array Analysis Methods*. 2018. URL: https://www.b-tu.de/fg-akustik/lehre/aktuelles/arraybenchmark (visited on 03/04/2018).

[20] E. Sarradj et al. "A Microphone Array Method Benchmarking Exercise using Synthesized Input Data". June 2017.

[21] C. J. Bahr et al. "A Comparison of Microphone Phased Array Methods Applied to the Study of Airframe Noise in Wind Tunnel Testing". *23rd AIAA/CEAS Aeroacoustics Conference*. Reston, Virginia: American Institute of Aeronautics and Astronautics, June 2017, pp. 1–19.

[22] A. Beck and M. Teboulle. "A Fast Iterative Shrinkage-Thresholding Algorithm for Linear Inverse Problems". *SIAM Journal on Imaging Sciences* 2.1 (Jan. 2009), pp. 183–202.

[23] N. Parikh and S. Boyd. "Proximal Algorithms". *Foundations and Trends in Optimization* 1 (Aug. 2013), pp. 123–231.

[24] O. Lylloff and E. Fernandez-Grande. *Noise Quantification with Beamforming Deconvolution: Effects of Regularization and Boundary Conditions - reproducible research steps*. 2018. URL: https://gitlab.windenergy.dtu.dk/ollyl/BeBeC18 (visited on 03/04/2018).

[25] F. Jacobsen and P. M. Juhl. *Fundamentals of general linear acoustics*. Wiley, 2013.

[26] E. Sarradj. "Three-Dimensional Acoustic Source Mapping with Different Beamforming Steering Vector Formulations". *Advances in Acoustics and Vibration* 2012.4 (2012), pp. 1–12. DOI: 10.1155/2012/292695.

[27] J. D. Maynard, E. G. Williams, and Y. Lee. "Nearfield acoustic holography: I. Theory of generalized holography and the development of NAH". *Journal of the Acoustical Society of America* 78 (1985), pp. 1395–1413.

[28] S. P. Boyd and L. Vandenberghe. *Convex optimization*. Cambridge university press, 2004.

[29] A. N. Tikhonov and V. Y. Arsenin. *Solutions of ILL-Posed Problems*. V.H. Winston & Sons, 1977.

[30] R. Tibshirani. "Regression Shrinkage and Selection via the Lasso". *Journal of the Royal Statistical Society. Series B (Methodological)* 58.1 (1996), pp. 267–288.

[31] A. Xenaki, E. Fernandez-Grande, and P. Gerstoft. "Block-sparse beamforming for spatially extended sources in a Bayesian formulation". *Journal of the Acoustical Society of America* 140.3 (Sept. 2016), pp. 1828–1838. DOI: 10.1121/1.4962325.

[32] Z. Chu et al. “Improvement of Fourier-based fast iterative shrinkage-thresholding deconvolution algorithm for acoustic source identification”. *Applied Acoustics* 123 (2017), pp. 64–72. DOI: 10.1016/j.apacoust.2017.03.010.

[33] P. Hansen, J. Nagy, and D. O’Leary. *Deblurring Images*. Society for Industrial and Applied Mathematics, 2006. DOI: 10.1137/1.9780898718874.

[34] J. Hald and J. J. Christensen. “Technical Review: Beamforming, No. 1”. *Brüel & Kjær* (2004).

[35] M. Aldeman et al. “Effects of Array Scaling and Advanced Beamforming on the Angular Resolution of Microphone Array Systems”. *Proceedings of the 6th Berlin Beamforming Conference*. 2016.